Preparation and characterisation of transition metal ions (Fe^{3+}, Mn^{2+}) doped CdO nanoparticles

Sara Abbas

Department of Chemistry,
Faculty of Science,
Beirut Arab University,
Debbieh, Lebanon
Email: sara.abbas_17@outlook.com

Hadi Basma* and Ramadan Awad

Department of Physics,
Faculty of Science,
Beirut Arab University,
Debbieh, Lebanon
Email: h.basma@bau.edu.lb
Email: hadibassma@gmail.com
Email: ramadan.awad@bau.edu.lb
*Corresponding author

Abstract: Pure, Fe^{3+}, and Mn^{2+} doped CdO nanoparticles were prepared by the wet co-precipitation technique. The crystal structure, vibrational modes, and morphology of the CdO nanoparticles were studied using X-ray powder diffraction (XRD), Fourier transmission infrared spectroscopy (FTIR), and transmission electron microscopy (TEM), respectively. XRD and TEM studies showed a reduction in the lattice parameters and particle size relative to the pure sample, respectively. The Cd-O vibration bands were detected by the FTIR analysis. The photoluminescence spectra showed deep-level blue and violet emissions attributed to Cd vacancies. The energy band-gap obtained from UV-visible spectroscopy (UV-Vis) was enhanced with the transition metal (T-M) ions substitutions. The M-H measurements showed a transition from diamagnetic to ferromagnetic behaviours as an effect of T-M substitution. Accordingly, this study reveals that the magneto-optical properties of CdO nanoparticles can be tuned by substitution with different transition metal ions, allowing for different applications such as magnetically recyclable photocatalysts and spin-valve devices.

Keywords: CdO nanoparticles; M-H hysteresis; photoluminescence; transition metal ions; UV-Vis spectroscopy.

Reference to this paper should be made as follows: Abbas, S., Basma, H. and Awad, R. (2022) 'Preparation and characterisation of transition metal ions (Fe^{3+}, Mn^{2+}) doped CdO nanoparticles', *Int. J. Nanoparticles*, Vol. 14, No. 1, pp.31–46.

Biographical notes: Sara Abbas is currently a PhD student at Beirut Arab University. She attained her BS degree in Chemistry and Master's in Physical Chemistry and Catalysis at Lebanese University. Her PhD thesis is about studying the synthesis, characterisation, and the effects of nano addition (CdO,

and transition metal ions (Fe^{3+}, Mn^{2+}) doped CdO nanoparticles) on the (Bi, Pb)-2212 superconductor. She has been teaching chemistry for nine years in an official school.

Hadi Basma completed his PhD in Materials as a part of a collaboration project between Beirut Arab University and the Lebanese Atomic Energy Commission (2016). He also holds a Master's in teaching Physics from the Lebanese University. He is an active professor, trainer, and researcher at Beirut Arab University. He represented the Ministry of Education and Higher Education in Lebanon and BAU in several international conferences including the US, India, Europe, and the MENA region. He has more than 20 publications in international peer-reviewed journals and has supervised several graduate students.

Ramadan Awad is the Dean of the Faculty of Science at Beirut Arab University completed his PhD as a Channel System between Alexandria University (Egypt) and Genoa University (Italy) in 1997. He worked in the field of high-temperature superconductivity Mercury – Thallium Cuprates. He was awarded the professor degree in 2007. He has supervised more than 80 masters and PhD students. His research interests are electrical and magnetic properties of solids, superconductivity, nano-oxides preparation, magnetic properties of nano-ferrite, and composite materials. He has more than 200 publications in the field of superconductivity and nano science and participated in more than twenty international conferences.

1 Introduction

The investigation of T-M doped CdO nanoparticles (NPS) has gained considerable attention during the last decade owing to their usage in a wide scope of applications such as transparent conducting oxides, phototransistors, photodiodes, solar cells, transparent electrodes, and gas sensors (Aydin et al., 2012; Zhao et al., 2002). CdO is classified as an n-type semiconductor. It has a direct band gap between 2.2 and 2.7 eV, a strong room-temperature excitonic binding energy, a weak electrical resistivity, and a strong transmission within the visible spectrum (Aswani et al., 2014). Research has validated that doping CdO with transition metal ions like Mn, Co, Ni, Cu, Zn, Ag, and Fe has enhanced the structural, optical, and magnetic properties of CdO NPS (Kumar et al., 2021; Dakhel et al., 2014; Dugan et al., 2020; Naser et al., 2020; Dakhel, 2020). This allowed for a vast range of optoelectronic applications.

Christuraj et al. (2020) have investigated the effect of Mn doping on CdO NPS prepared by the co-precipitation method. The XRD results of CdO NPS showed an increase in the crystallise size with Mn doping, without an observable shift in the positions of the diffraction peaks. Specific capacitance measurements showed an enhancement with Mn doping. Kumar et al. (2015) reported that Mn doping reduced the crystallite size of CdO NPS, leading to an increase in the energy band gap, and a decrease in the magnetic coercivity of the room temperature ferromagnetic behaviour of CdO NPS. Tawfik et al. (2017) explored the effect of Fe doping on CdO NPS. The particle size was reduced monotonically with increasing the Fe doping. Pure CdO revealed ferromagnetic behaviour but anti-ferromagnetism was present in all Fe-doped samples and was associated with anisotropic change and structural dislocations.

In this work, we aim to compare the magneto-optical effect of TM substitutions of CdO NPS prepared under the same conditions and particle size distribution. The results obtained for pure, Fe^{3+} and Mn^{2+} substituted CdO NPS accumulated by the co-precipitation method at PH = 12 and T = 650°C are reported. Fe^{3+} and Mn^{2+} were chosen because they are stable transition metals. They both have an ionic radius smaller than the radius of Cd^{2+} allowing them to substitute Cd^{2+} in the CdO matrix without causing much lattice deformation. Furthermore, previous research (Tawfik et al., 2017; Dakhel et al., 2014; Christuraj et al., 2020; Kumar et al., 2015) has shown the effect of Mn^{2+} and Fe^{3+} doping in changing the magnetic nature of CdO NPS allowing for different applications.

The effect of transition metal ions substitution on the structural, optical, and magnetic properties is investigated. The Structural properties including the crystal structure, crystalline size, morphology, and functional groups of the prepared NPS are studied by using X-ray diffraction (XRD), transmission electron microscopy (TEM), and Fourier transform infrared (FTIR) spectroscopy. While the optical properties are investigated by using ultraviolet-visible absorption spectroscopy (UV) and photoluminescence spectroscopy (PL), and. Finally, the magnetic properties of the prepared NPS are studied by tracing room temperature magnetic hysteresis curves.

2 Materials and methods

Samples of pure CdO, $Cd_{0.95}Fe_{0.05}O$, and $Cd_{0.95}Mn_{0.05}O$ NPS were prepared by the following procedure: The first sample: 15g of $CdCl_2$ were dissolved in 32.8 ml of distilled water. Second sample: 24.64 g of $CdCl_2$ were dissolved in 50 ml of distilled water mixed with 0.35 g of $MnCl_2$ that was dissolved in 6.8 ml of distilled water. Third sample: 24.24 g of $CdCl_2$ were dissolved in 50 ml of distilled water mixed with 0.75 g of $FeCl_3$ that was dissolved in 5.8 ml of distilled water. Each sample was stirred with 2.9 g of EDTA for 30 minutes using a magnetic stirrer to reduce agglomeration. Then, the titration method was performed for the three samples with the obtained solution using 2 M NaOH (m = 8 g) until pH = 12 then was heated for two hours at T = 80°C during stirring. The titration is performed to initiate the nucleation of the CdO NPS. The three samples were then filtered using distilled water to remove impurities and spectator ions. They were dried for 16 hours using the furnace to evaporate excess water, then crushed with a mortar. Finally, the calcination method was performed for the three samples at T = 650°C for three hours. During the calcination process, the O-H bonds are broken down and the cadmium hydroxide is transformed into Cadmium oxide. Then the crystallisation of cadmium oxide NPS is formed. It should be noted that the values of PH = 12 and T = 650°C, were chosen because the preparation and the characteristics of the pure cadmium oxide NPS are optimal at these conditions, based on a previous study (Abbas et al., 2021) that investigated the effect of PH and calcination temperature on the formation and characterisation of pure CdO NPS.

The crystal structure of the NPS was inspected by applying X-ray powder diffraction using the Bruker D8 advance powder diffractometer with Cu-K_α radiation (λ = 1.54056 A°) in the range of $25° \leq 2\theta \leq 75°$. TEM images were obtained by using the Jeol transmission electron microscope JEM 100CX, operated at 80kV. The FTIR spectrum was determined by an FTIR 8400S Shimadzu. The optical properties were characterised by using the ultraviolet-visible near-infrared (NIR) spectrophotometer V-670 operating in

absorption mode at a wavelength of 4,000 nm–350 nm at room temperature by measuring spectral diffuse reflectance spectroscopy (DRS). The room temperature photoluminescence (PL) spectra were measured using the FP-8300 spectrofluorometer. To examine the magnetic properties a vibrating sample magnetometer (VSM), Lakeshore 7410, was used up to a field of 20,000 G.

3 Results and discussion

3.1 XRD results

Figure 1 depicts the XRD patterns of CdO, $Cd_{0.95}Fe_{0.05}O$, and $Cd_{0.95}Mn_{0.05}O$. All three spectra show high crystallinity with strong reflection peaks located at 2θ = 33.01°, 38.31°, 55.3°, 65.93° and 69.28° and indexed to the planes (111), (200), (220), (311), and (222) respectively by using the standard found in JCPDS Card No. 65-2908 (Tadjarodi and Imani, 2011). The XRD patterns confirm the formation of cubic NPS having a space group Fm3m. The spectra of the doped samples have not shown any additional phase, confirming the complete and successful substitution of Cd^{2+} by the transition metals ions.

The lattice parameter 'a' of the cubic structure is evaluated by applying the Rietveld refinement using the MAUD software, as shown in Figure 2. The values of 'a' are listed in Table 1. The values of 'a' show a slight decrease with Fe^{3+} and Mn^{2+} substitution. This is attributed to the shrinkage of the crystal lattice due to the difference in ionic radii between the dopant ions and the larger Cd^{2+} ions (Kumar et al., 2021; Bhukkal and Ahlawat, 2020). The values of the bond length are also calculated and shown in Table 1. They show similar behaviour to 'a' with the transition metal substitution.

The average crystallite size 'D' was determined using the modified Debye-Scherer's formula

$$\ln\beta = \ln\left(\frac{1}{\cos\theta}\right) + \ln(k\lambda / D). \tag{1}$$

where D is the crystallite size, λ is the X-ray wavelength, β is the full width at half the maximum of the diffraction peak, and θ is the Bragg diffraction angle of corresponding peaks (Gupta et al., 2017).

The plots of lnβ versus ln(1/cosθ) are shown in Figure 3 The values of D obtained from the y-intercept of the graphs are listed in Table 1.

Table 1 List of structural parameters and energy band gap for pure CdO, $Cd_{0.95}Fe_{0.05}O$, and $Cd_{0.95}Mn_{0.05}O$ NPS

Sample	*a (Å)*	D_{XRD} *(nm)*	D_{TEM} *(nm)*	*I*	*ℓ (Å)*	E_g *(eV)*
CdO	4.6996	41.24	68.97	1.688	2.349	2.63
$Cd_{0.95}Fe_{0.05}O$	4.6976	40.87	42.01	1.01	2.340	3.05
$Cd_{0.95}Mn_{0.05}O$	4.6984	39.79	67.48	1.721	2.348	3.55

The data shows the decrease in the crystallite size from 41.4 nm for pure CdO to 40.87 nm for ($Cd_{0.95}Fe_{0.05}O$) and 39.4 nm for ($Cd_{0.95}Mn_{0.05}O$). This is assigned to the difference between the ionic radii of Cd^{2+} (0.95 A°), Fe^{3+} (0.63 A°), and Mn^{2+} ion (0.83 A°) that causes lattice distortion and induces internal stresses in the CdO matrix

which consequently affects the growth kinematics and nucleation (Kumar et al., 2016; Gupta et al., 2008).

Figure 1 XRD patterns of pure CdO, $Cd_{0.95}Fe_{0.05}O$ and $Cd_{0.95}Mn_{0.05}O$ NPS (see online version for colours)

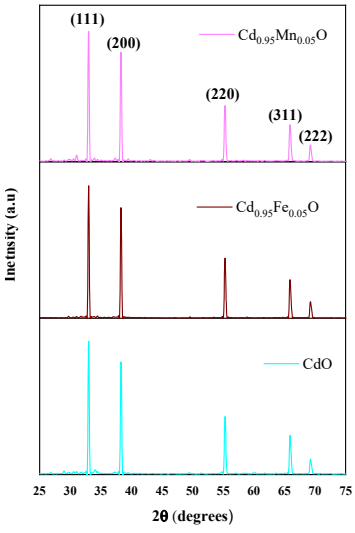

Figure 2 Reitveld refinement of the XRD spectrum of pure CdO, $Cd_{0.95}Fe_{0.05}O$, and $Cd_{0.95}Mn_{0.05}O$ NPS using MAUD software (see online version for colours)

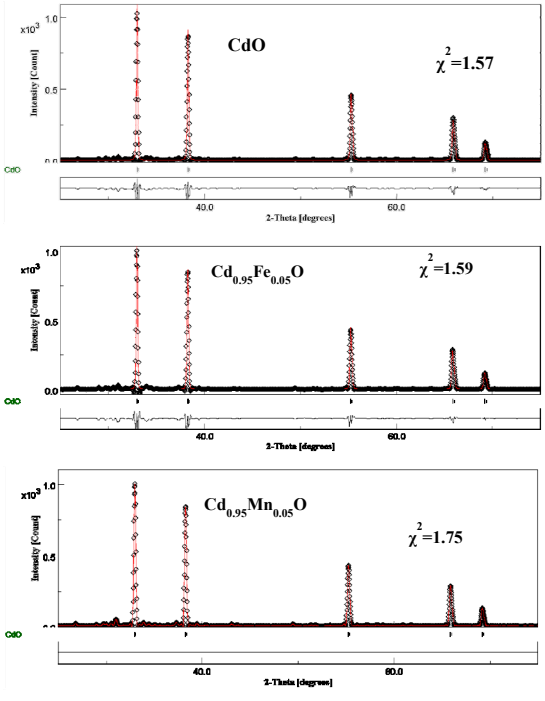

Figure 3 ln(1/β) versus ln(cosθ) plots for pure CdO, $Cd_{0.95}Fe_{0.05}O$ and $Cd_{0.95}Mn_{0.05}O$ NPS (see online version for colours)

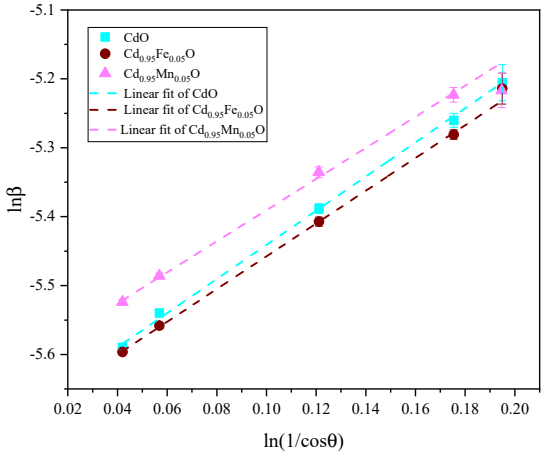

3.2 Transmission electron microscopy

Figures 4(a)–4(c) shows the TEM images for pure Fe^{3+}, and Mn^{2+} substituted CdO NPS, respectively. The particle size histograms obtained using the ImageJ software are also depicted. The TEM images confirm the successful preparation of the samples at the nanoscale. The particles are nearly homogenous and spherical. The average particle sizes (D_{TEM}) are shown in Table 1. These are larger than the crystallite size obtained from XRD measurements (D_{XRD}).

Using the values of D_{XRD} and D_{TEM} we can calculate the crystallinity index, I where

$$I = \frac{D_{TEM}}{D_{XRD}}. \tag{2}$$

The values of I are listed also in Table 1, where I decrease for Fe^{3+} doped sample and increases for the Mn^{2+} doped sample relative to the pure CdO sample. The values of I are correlated to the degree of agglomeration of the particles.

3.3 FTIR spectra analysis

The study of the vibrational modes was performed using FTIR spectroscopy. The graphs of Figure 5 show the FTIR spectra of pure CdO, $Cd_{0.95}Mn_{0.05}O$, and $Cd_{0.95}Fe_{0.05}O$ NPS. No vibrational bands corresponding to secondary phases were detected, which is compatible with the XRD results. The broad and sharp bands observed between 3,460.02 cm^{-1}, 3,446.12 cm^{-1} and 1,635.50 cm^{-1} are the characteristics of the hydroxyl (OH) group. The first corresponds to the O-H stretching and the second corresponds to the H-O-H bending vibration (Basma et al., 2019). The peaks at approximately 2,365 cm^{-1} correspond to the O = C = O vibration mode (Al Boukhari et al., 2020). The band at 1,440 results from the symmetric vibrations of acetate complex COO − present in the precursors (Yadav et al., 2016).

Figure 4 TEM micrographs and corresponding particle size histograms of pure CdO, $Cd_{0.95}Fe_{0.05}O$, and $Cd_{0.95}Mn_{0.05}O$ NPS, respectively (see online version for colours)

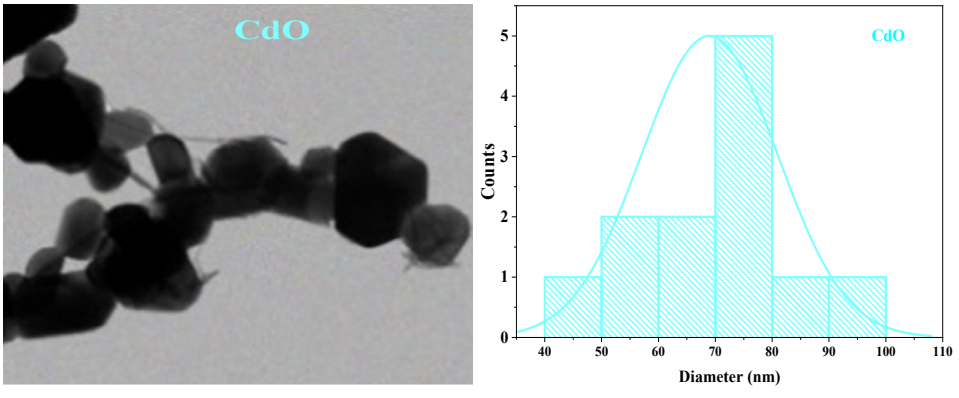

(a)

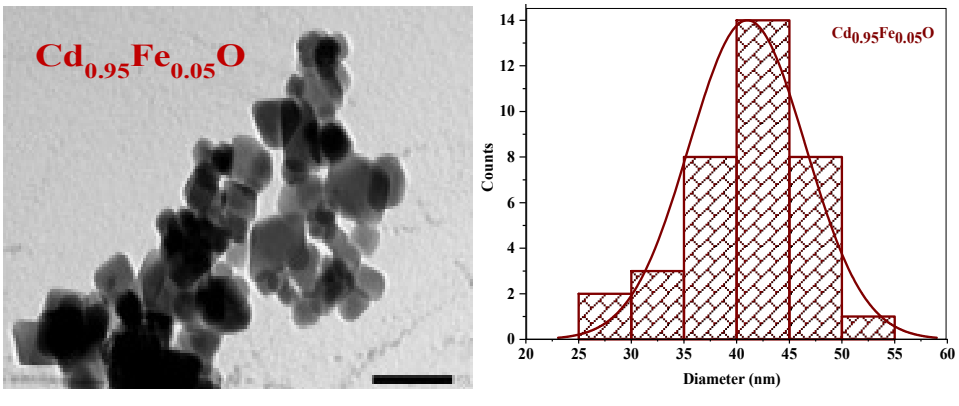

(b)

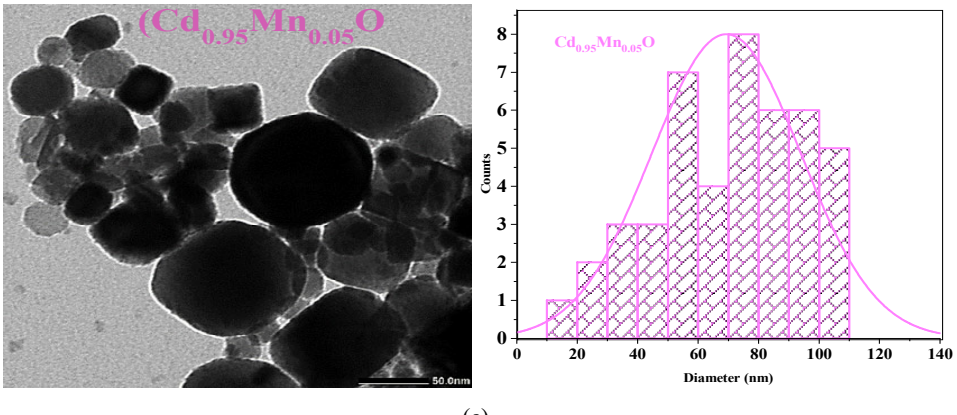

(c)

The bands between 500 cm^{-1} and 900 cm^{-1} correspond to CdO (Ranjithkumar et al., 2016). As shown in Figure 5(b), the most intense peaks, at 650–670 cm^{-1}, correspond to Cd-O asymmetric stretching vibrations (Bhukkal and Ahlawat, 2020) and the peaks at

540–570 cm^{-1} correspond to Cd-O bending vibrations (Anandhan and Kumar, 2015), while the peaks at 875 cm^{-1} correspond to Cd-OH bending (Bhukkal et al., 2020). The amplitude and the wave number of the bands corresponding to Cd-O vibrations vary significantly with Fe^{3+} and Mn^{2+} substitution. This signifies the successful incorporation of the substituting ions inside the crystal lattice, which perturbs the crystal structure. This is compatible with the XRD findings the showed a variation of lattice parameter and crystallite size as a result of this ionic substitution.

Figure 5 FTIR spectra of pure CdO, $Cd_{0.95}Fe_{0.05}O$ and $Cd_{0.95}Mn_{0.05}O$ NPS at different wavenumber range (see online version for colours)

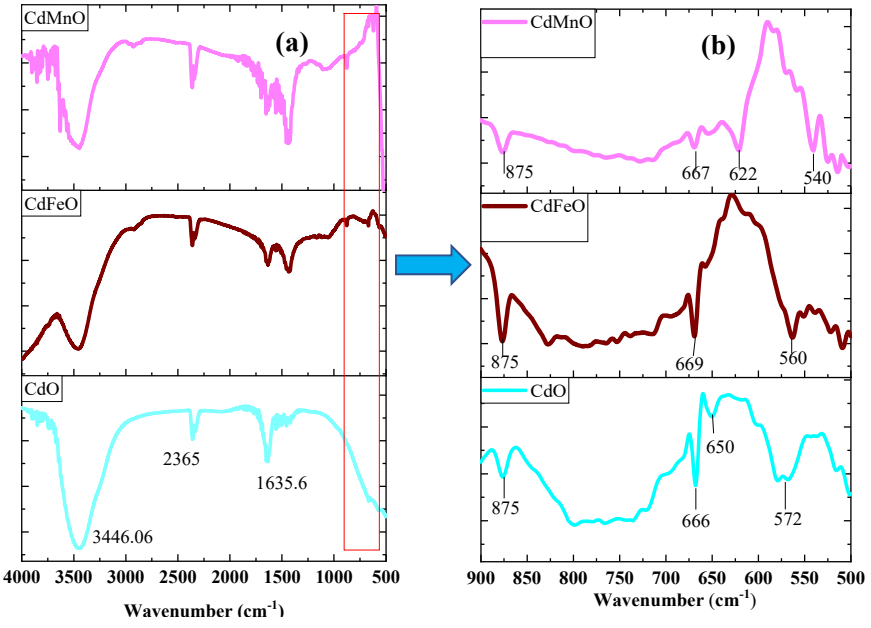

3.4 *Photoluminescence studies*

Figures 6(a)–6(c) shows the room temperature PL emission spectra of pure, Fe^{3+} and Mn^{2+} doped CdO NPs, respectively. The emission spectrum of pure CdO consists of an ultraviolet peak positioned at 390 nm and four visible peaks positioned at 425, 465, 503, and 616 nm. The ultraviolet emission results from near-band-edge emission (NBE) due to the transitions occurring because of the recombination of excitons (Kisan et al., 2014). On the other hand, the four visible emissions which are also denoted by deep-level emissions (DLE) usually result from structural defects encouraged by thermal treatment during preparation, and deviation from stoichiometric proportions of the samples. Among all defects, Cadmium vacancies (Cd_i) and oxygen interstitials (O_i) are the most effective (Diallo et al., 2018). The emission observed at 425nm is possibly due to the transitions of trapped electrons from Cd_i to V_b (Gandhi and Wu, 2017). The blue emission peak at 460 nm is attributed to the surface trap emission or deep-level emission (Kumar et al., 2016; Asenjun and Alemi, 2019) from Cd interstitial vacancies and oxygen vacancies. The green and orange emission peaks, that appear weakly at 503 and 620 nm, respectively are related to O_i and Cd vacancies (Karthikeyan et al., 2016; Liu et al., 2004).

Figure 6 (a) (b) (c) PL emission spectra with deconvolution plots of pure CdO, $Cd_{0.95}Fe_{0.05}O$, and $Cd_{0.95}Mn_{0.05}O$ NPS, respectively (d) shows CIE chromaticity diagram of pure CdO, $Cd_{0.95}Fe_{0.05}O$ and $Cd_{0.95}Mn_{0.05}O$ NPS (see online version for colours)

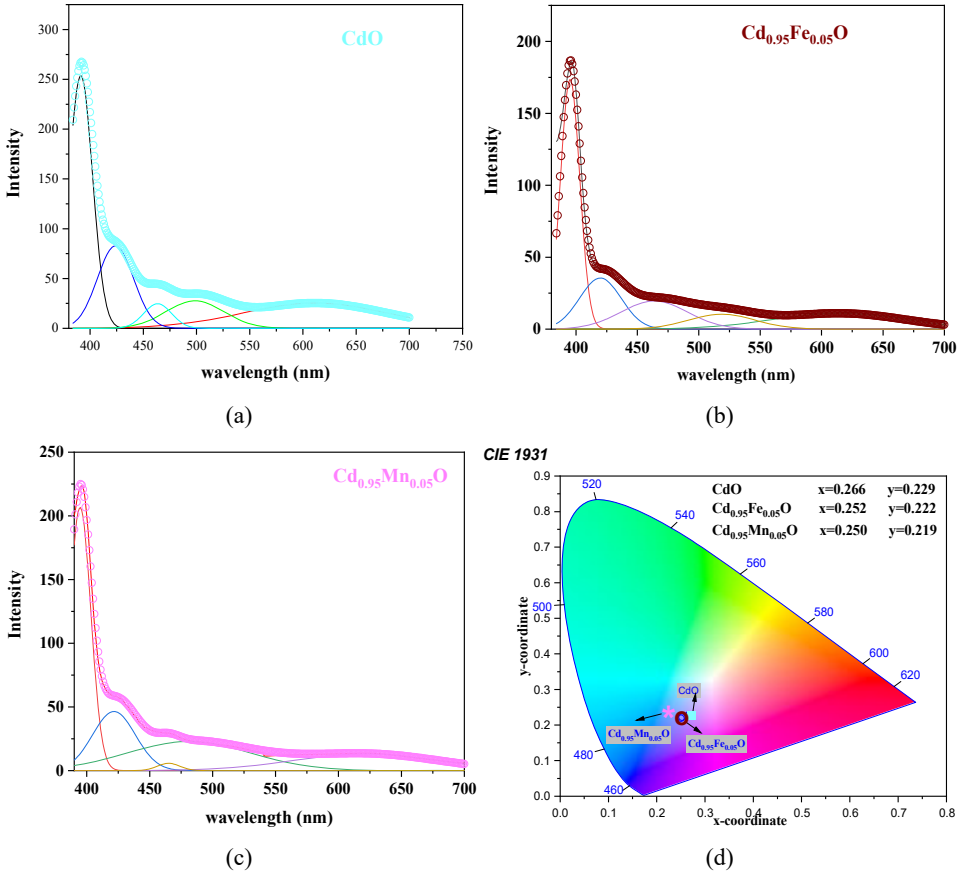

Table 2 PL peak positions and intensities of prepared pure CdO, $Cd_{0.95}Fe_{0.05}O$, and $Cd_{0.95}Mn_{0.05}O$ NPS

	Peak position (nm)					*Peak height intensity*				
	1	*2*	*3*	*4*	*5*	*1*	*2*	*3*	*4*	*5*
CdO	390.85	425.96	464.45	502.57	614.93	251.81	83.05	23.82	28.38	28.57
$Cd_{0.95}Fe_{0.05}O$	396.14	419.22	466.46	525.74	615.84	172.65	34.98	20.48	11.64	13.97
$Cd_{0.95}Mn_{0.05}O$	394.96	422.50	465.54	481.51	614.84	204.94	46.74	6.35	22.46	16.16

Compared to the pure CdO, the intensity of all PL emissions decreases for the Fe^{3+} and Mn^{2+} substituted CdO NPs. This variation is illustrated in Table 2. This decrease in PL intensities is linked to the enhancement of Cd vacancies on the crystal surface, which generates a lower electron population at the level of the valence band and suppresses the process of recombination of electrons and holes (Gandhi and Wu, 2017).

The slight shift (red or violet) in the position of the peaks can be endorsed to the variation of the particle size as calculated using TEM and XRD measurements.

For further investigation of the optical (luminescent) properties of the NPS, CIE 1931 Chromaticity coordinates were also calculated from the emission spectrum (Aswani et al., 2014). Based on the spectral power distribution of the radiations emitted by each sample, the colour coordinates (x, y) were calculated and are depicted in Figure 6(d). The colour coordinates of all three samples are located in the blue-violet region.

3.5 Ultraviolet-absorption spectroscopy

The optical absorption spectra of pure CdO and Mn^{2+}, Fe^{3+} ions doped CdO NPS are shown in Figure 7. These spectra show the UV absorbance spectrum of the pure CdO NPs at 227 nm. A blue shift of the absorption edge with Fe^{3+} and Mn^{2+} substitutions is observed.

Figure 7 Absorbance versus wavelength for pure CdO, $Cd_{0.95}Fe_{0.05}O$, and $Cd_{0.95}Mn_{0.05}O$ NPS (see online version for colours)

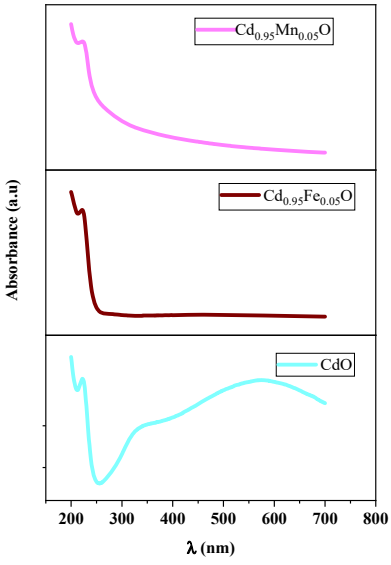

The Tauc plots shown in Figures 8(a)–8(c) represent the dependence of $(\alpha h\upsilon)^2$ on the photon energy hυ. The linear part of the plots is extrapolated and its intersection with the x-axis allows to determine the value of the energy band gap (E_g). The values of E_g are depicted in Table 1. The pure CdO has a direct energy gap value of 2.63 eV, and the value is increased to 3.05 eV and 3.55 eV for Fe^{3+} and Mn^{2+} doped CdO NPS, respectively. Moreover, this blue shift in band gap can be attributed to the Burstein-Moss effect (Hymavathi et al., 2015).

According, to the Burstein-Moss effect, the substitution with T-M leads to an increase in the carrier concentrations, and this might shift the Fermi level towards the conduction band leading to an increase in the optical band gap. These results support our assumption that the Mn^{2+} and Fe^{3+} ions have successfully integrated into the CdO crystal structure and successfully substituted the Cd^{2+} sites. The Burstein-Moss effect was evident for CdO thin films doped by Cu (Menazea et al., 2019), Mn (Kasirajan et al., 2021), and Te (Sönmezoğlu et al., 2013).

Figure 8 $(\alpha h\upsilon)^2$ versus the photon energy hυ of pure CdO, $Cd_{0.95}Fe_{0.05}O$, and $Cd_{0.95}Mn_{0.05}O$ NPS, respectively (see online version for colours)

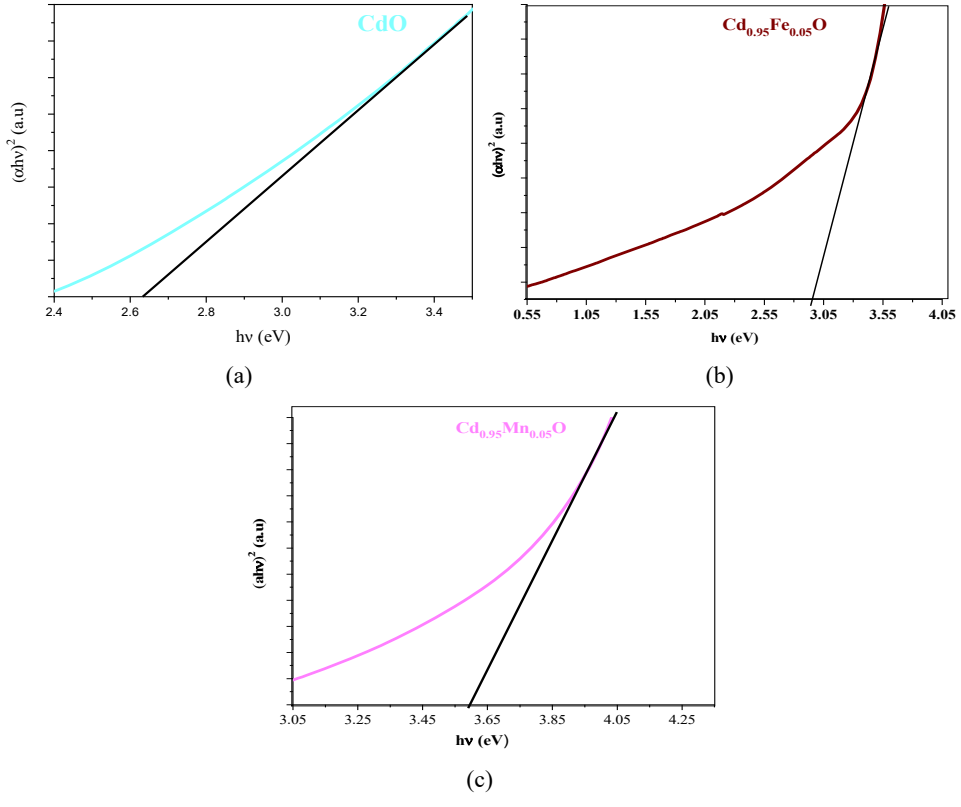

3.6 M-H studies

Figures 9(a)–9(c) shows the room temperature magnetic hysteresis (M-H) loops for pure CdO, $Cd_{0.95}Fe_{0.05}O$, and $Cd_{0.95}Mn_{0.05}O$ NPS, respectively.

For pure CdO, the plot of Figure 9(a) confirms that pure CdO has an intrinsic diamagnetic response with a negative slope, accompanied by a very weak d^0FM component. This weak Ferromagnetism might be attributed to oxygen vacancies that enhance the magnetic medium for spin-spin interactions (Dakhel, 2018). The diamagnetism behaviour in pure CdO NPS has been assigned to the fact that d-electrons are completely paired (Chandiramouli and Jeyaprakash, 2013).

The Fe^{3+} substituted CdO NPS demonstrated very narrow hysteresis loops, which are characteristic of soft magnetic materials. These loops show a combination of paramagnetic and weak ferromagnetism at lower fields as shown in Figure 9(b). The weak ferromagnetic signature is shown in the inset of Figure 9(b).

This observed ferromagnetism is attributed to the rise of ferromagnetic exchange coupling between the spins and augmentation of spin concentrations due to the integration of Fe^{3+} ions in the lattice (Dakhel, 2014). It has been reported (Beltrán et al., 2015) that substitution with Fe^{3+} contributes to the enhancement of ferromagnetism by

increasing the surface defects of the crystal structure such as the formation of single charged oxygen vacancies, and oxygen-ended polar terminations.

Figure 9 M-H hysteresis curves for pure CdO, $Cd_{0.95}Fe_{0.05}O$, and $Cd_{0.95}Mn_{0.05}O$ NPS, respectively (see online version for colours)

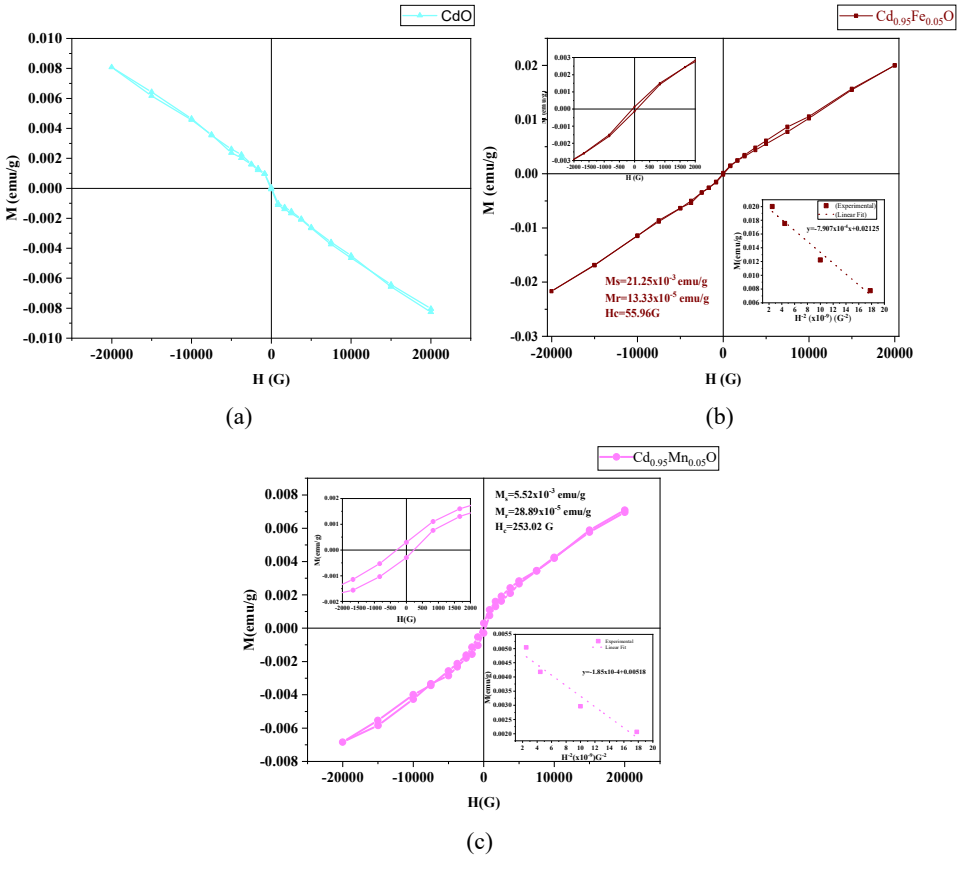

Notes: The insets show the plots of M versus $1/H^2$ and zoom to the hysteresis at lower fields.

These mainly superficial defects altered the electronic structure causing the observed ferromagnetism.

This enhanced ferromagnetism is useful in photocatalytic degradation applications discussed in PL emission. As it allows the photocatalyst ($Cd_{0.95}Fe_{0.05}O$) to be separated and recycled by applying an external magnetic field. This assures sustainability making them cost-effective and environmentally friendly.

The values of the saturation magnetisation were calculated by using the law of approach to saturation based on the model developed by Stoner and Wolhfrath (Tannous and Gieraltowski, 2008):

$$M(H) = M_S\left[1 - \frac{A}{H} - \frac{B}{H^2}\right] + \chi_P H$$

where A represents the inhomogeneity parameter, B represents the anisotropy parameter and χ_P represents the high field differential susceptibility.

The plots of M versus $1/H^2$ for $10 \leq H \leq 15$ KG shown in the insets of Figures 9(b) and 9(c) show a linear dependence. This allows neglecting the constants A and χ_P (Fang et al., 1998).

The values of M_r and H_c, the retentivity, and coercivity were also determined from the hysteresis loops and are also shown in the insets of Figures 9(b) and 9(c).

The Mn^{2+} doped CdO NPS show also very narrow hysteresis loops, with a reduced saturation magnetisation as compared to the Fe^{3+} doped sample and an enhanced coercivity. Previous studies (Wolff et al., 1996; Coey et al, 2005; Durst et al., 2002; Rao et al., 2015) have suggested that the bound magnetic polaron (BMP) model might explain the observed ferromagnetism in transition metal-doped metal oxides. The BMP model assumes an exchange interaction between the spin of the Mn^{2+} ions and the spin of the localised holes resulting from Zn vacancies. Furthermore, other studies (Kamran et al., 2014) argued that the observed ferromagnetic behaviour might be due to the changes in the size and structure of the spin distribution induced by Mn^{2+} doping within the distorted band structure.

The substitution by Mn^{2+} induces changes in particle shapes and sizes. The coercivity is proportional to the effective crystalline anisotropy which is related to the shape anisotropy, size anisotropy, surface anisotropy, and the isotropy constant related to interactions among magnetic particles (Caizer and Stefanescu, 2003). The TEM micrograph [Figure 4(c)] shows a broad particle size distribution ranging from 20 to 120 nm and a difference in the shapes of the NPS. This shape anisotropy might explain the increase in the coercivity value of $Cd_{0.95}Mn_{0.05}O$ NPS (Taufik et al., 2018). CdO ferromagnetic NPS with elevated coercivity might find applications as pinning layers in spin valves (Tawfik et al., 2017).

4 Conclusions

Pure, Fe^{3+}, and Mn^{2+} substituted CdO was successfully prepared. The formation of a single-phase structure and the complete incorporation of the TM ions in the lattice structure were confirmed by XRD, TEM, and FTIR analysis. The deep level emissions detected in the photoluminescence spectra showed deep level blue and violet emissions corresponding to Cd vacancies. The energy band gap was enhanced as a result of the T-M ions substitutions. A shift of the magnetic behaviour from diamagnetic to ferromagnetic was observed with an enhanced saturation magnetisation and a diminished coercivity for $Cd_{0.95}Fe_{0.05}O$. Whereas for $Cd_{0.95}Mn_{0.05}O$ NPS, a shift to an antiferromagnetic behaviour was observed. This allows for interesting magneto-optical applications.

References

Abbas, S., Basma, H., Al Boukhari, J. and Awad, R. (2021) 'Characterization of CdO nanoparticles prepared by co-precipitation method under different pH and calcination temperatures', *Applied Physics A*, Vol. 127, No. 7 [online] https://doi.org/10.1007/s00339-021-04669-5.

Al Boukhari, J., Khalaf, A. and Awad, R. (2020) 'Structural analysis and dielectric investigations of pure and rare earth elements (Y and Gd) doped NiO nanoparticles', *Journal of Alloys and Compounds*, April, Vol. 820, No. 0925-8388, p.153381.

Anandhan, K. and Kumar, R.T. (2015) 'Synthesis, FTIR, UV-Vis and photoluminescence characterizations of triethanolamine passivated CdO nanostructures', *Spectrochimica Acta Part A: Molecular and Biomolecular Spectroscopy*, October, Vol. 149, No. 1386-1425, pp.476–480.

Asenjun, A.K. and Alemi, A. (2019) 'Enhancement of photodegradation efficiency, photoluminescence quantum yield, and magnetization in highly Yb^{3+}-doped CdO nanoparticles synthesized via sol-gel method', *Research on Chemical Intermediates*, 8 May, Vol. 45, No. 5, pp.3183–3198.

Aswani, T., Babu, B., Manjari, V.P., Stella, R.J., Rao, G.T., Krishna, C.R. et al. (2014) 'Synthesis and spectral characterizations of trivalent ions (Cr^{3+}, Fe^{3+}) doped CdO nanopowders', *Spectrochimica Acta – Part A: Molecular and Biomolecular Spectroscopy*, Vol. 121, No. 1386-1425, pp.544–150.

Aydin, C., Al-Hartomy, O.A., Al-Ghamdi, A.A., Al-Hazmi, F., Yahia, I.S., El-Tantawy, F. et al. (2012) 'Controlling of crystal size and optical band gap of CdO nanopowder semiconductors by low and high Fe contents', *Journal of Electroceramics*, Vol. 29, No. 2, pp.155–162.

Basma, H., Rahal, H.T., Al-Mokdad, F., Romie, M. and Awad, R. (2019) 'Unusual magnetic behavior of nanosized ZnO doped with Mo^{6+}', *Materials Research Express*, 3 April, Vol. 6, No. 7, No. 7, p.075001.

Beltrán, J.J., Barrero, C.A. and Punnoose, A. (2015) 'Understanding the role of iron in the magnetism of Fe doped ZnO nanoparticles', *Physical Chemistry Chemical Physics*, 15 June, Vol. 17, No. 23, pp.15284–15296.

Bhukkal, C. and Ahlawat, R. (2020) Cu^{2+}-Mn^{2+}-Co-doped CdO nanocrystallites: comprehensive research on phase, morphology and optoelectronic properties', *Research on Chemical Intermediates*, 1 September, Vol. 46, No. 9, pp.4211–4232.

Bhukkal, C., Chauhan, M. and Ahlawat, R. (2020) 'Synthesis, structural and enhanced optoelectronic properties of Cd(OH)2/CdO nanocomposite', *Physica B: Condensed Matter.*, April, Vol. 582, No. 0921-4526, p.411973.

Caizer, C. and Stefanescu, M. (2003) 'Nanocrystallite size effect on σs and Hc in nanoparticle assemblies', *Physica B: Condensed Matter.*, Vol. 327, No. 1, pp.129–134.

Chandiramouli, R. and Jeyaprakash, B.G. (2013) 'Review of CdO thin films', *Solid State Sciences*, Vol. 16, No. 1293-2558, pp.102–110, Elsevier Masson SAS.

Christuraj, P., Raja, M.D., Pari, S., Kumar, G.S. and Shankar, V.U. (2020) 'Synthesis of Mn doped CdO nanoparticles by co-precipitation method for supercapacitor applications', *Materials Today: Proceedings*, September.

Coey, J.M.D., Venkatesan, M. and Fitzgerald, C.B. (2005) 'Donor impurity band exchange in dilute ferromagnetic oxides', *Nature Materials*, Vol. 4, No. 2, pp.173–179.

Dakhel, A.A. (2018) 'Structural, optical, and magnetic studies of iodine-doped CdO nanopowders and films', *Journal of Sol-Gel Science and Technology*, 17 February, Vol. 85, No. 2, pp.311–317.

Dakhel, A.A. (2020) 'Generation of magnetic properties in degenerated Ni and Ga codoped CdO nanocrystals', *Journal of Superconductivity and Novel Magnetism*, 1 June, Vol. 33, No. 6, pp.1871–1877.

Dakhel, A.A., El-Hilo, M. and Bououdina, M. (2014) 'Ferromagnetic properties of Cu- and Fe-codoped nanocrystalline CdO powders: annealing in hydrogen promote long-range ferromagnetic order', *Advanced Powder Technology*, 1 November, Vol. 25, No. 6, pp.1839–1844.

Diallo, A., Kaviyarasu, K., Ndiaye, S., Mothudi, B.M., Ishaq, A., Rajendran, V. et al. (2018) 'Structural, optical and photocatalytic applications of biosynthesized NiO nanocrystals', *Green Chemistry Letters and Reviews*, 3 April, Vol. 11, No. 2, pp.166–175.

Dugan, S., Koç, M.M. and Coşkun, B. (2020) 'Structural, electrical and optical characterization of Mn doped CdO photodiodes', *Journal of Molecular Structure*, 15 February, Vol. 1202, No. 0022-286, p.127235.

Durst, A.C., Durst, A.C., Bhatt, R.N. and Wolff, P.A. (2002) 'Bound magnetic Polaron interactions in insulating doped diluted magnetic semiconductors', *Physical Review B – Condensed Matter and Materials Physics*, Vol. 65, No. 23, pp.2352051–23520510.

Fang, H.C., Yang, Z., Ong, C.K., Li, Y. and Wang, C.S. (1998) 'Preparation and magnetic properties of (Zn-Sn) substituted barium hexaferrite nanoparticles for magnetic recording', *Journal of Magnetism and Magnetic Materials*, August, Vol. 187, No. 1, pp.129–135.

Gandhi, A. and Wu, S. (2017) 'Strong deep-level-emission photoluminescence in NiO nanoparticles', *Nanomaterials*, 22 August, Vol. 7, No. 8, p.231.

Gupta, R.K., Ghosh, K., Patel, R., Mishra, S.R. and Kahol, P.K. (2008) 'Structural, optical and electrical properties of In doped CdO thin films for optoelectronic applications', *Materials Letters*, July, Vol. 62, No. 19, pp.3373–3375.

Gupta, V.K., Fakhri, A., Tahami, S. and Agarwal, S. (2017) 'Zn doped CdO nanoparticles: structural, morphological, optical, photocatalytic and anti-bacterial properties', *Journal of Colloid and Interface Science*, 15 October, Vol. 504, No. 0021-9797, pp.164–170.

Hymavathi, B., Kumar, B.R. and Rao, T.S. (2015) 'Investigations on physical properties of nanostructured Cr doped CdO thin films for optoelectronic applications', *Procedia Materials Science*, Vol. 10, pp.285–291.

Kamran, M.A., Liu, R., Shi, L.J., Li, Z.A., Marzi, T., Schöppner, C. et al. (2014) 'Tunable emission properties by ferromagnetic coupling Mn(II) aggregates in Mn-doped CdS microbelts/ nanowires', *Nanotechnology*, Vol. 25, No. 38, p.385201.

Karthikeyan, B., Pandiyarajan, T., Hariharan, S. and Ollakkan, M.S. (2016) 'Wet chemical synthesis of diameter tuned NiO microrods: microstructural, optical and optical power limiting applications', *CrystEngComm.*, Vol. 18, No. 4, pp.601–607.

Kasirajan, K., Anasthasiya, A.N.A., Aldossary, O.M., Ubaidullah, M. and Karunakaran, M. (2021) 'Structural, morphological, optical and enhanced photodetection activities of CdO films: an effect of Mn doping', *Sensors and Actuators, A: Physical*, Vol. 319, No. 1, p.112531.

Kisan, B., Shyni, P.C., Layek, S., Verma, H.C., Hesp, D., Dhanak, V. et al. (2014) 'Finite size effects in magnetic and optical properties of antiferromagnetic NiO nanoparticles', *IEEE Transactions on Magnetics*, January, Vol. 50, No. 1, pp.1–4.

Kumar, B.R., Prasad, K.H., Kasirajan, K., Karunakaran, M., Ganesh, V., Bitla, Y. et al. (2021) 'Enhancing the properties of CdO thin films by co-doping with Mn and Fe for photodetector applications', *Sensors and Actuators, A: Physical*, 1 March, Vol. 319, No. 0924-4247, p.112544.

Kumar, S., Layek, S., Yashpal, M. and Ojha, A.K. (2015) 'Room temperature ferromagnetism in undoped and Mn doped CdO nanostructures', *Journal of Magnetism and Magnetic Materials*, 26 June, Vol. 393, No. 0304-8853, pp.555–61.

Kumar, S., Ojha, A.K. and Walkenfort, B. (2016) 'Cadmium oxide nanoparticles grown in situ on reduced graphene oxide for enhanced photocatalytic degradation of methylene blue dye under ultraviolet irradiation', *Journal of Photochemistry and Photobiology B: Biology*, June, Vol. 159, No. 1011-1344, pp.111–119.

Liu, X., Wu, X., Cao, H. and Chang, R.P.H. (2004) 'Growth mechanism and properties of ZnO nanorods synthesized by plasma-enhanced chemical vapor deposition', *Journal of Applied Physics*, 15 March, Vol. 95, No. 6, pp.3141–3147.

Menazea, A.A., Mostafa, A.M. and Al-Ashkar, E.A. (2019) 'Impact of CuO doping on the properties of CdO thin films on the catalytic degradation by using pulsed-laser deposition technique', *Optical Materials*, December, Vol. 100, p.109663 [online] https://doi.org/10.1016/ j.optmat.2020.109663.

Naser, D.K., Abbas, A.K. and Aadim, K.A. (2020) 'Zeta potential of Ag, Cu, ZnO, CdO and Sn nanoparticles prepared by pulse laser ablation in liquid environment', *Iraqi Journal of Science*, Vol. 61, No. 10, pp.2570–2581.

Ranjithkumar, R., Irudayaraj, A.A., Jayakumar, G., Raj, A.D., Karthick, S. and Vinayagamoorthy, R. (2016) 'Synthesis and properties of CdO and Fe doped CdO nanoparticles', in *Materials Today: Proceedings*, Elsevier Ltd, pp.1378–1382.

Rao, G.T., Stella, R.J., Babu, B., Ravindranadh, K., Venkata Reddy, C., Shim, J. et al. (2015) 'Structural, optical and magnetic properties of Mn^{2+} doped ZnO-CdS composite nanopowder', *Materials Science and Engineering B: Solid-State Materials for Advanced Technology*, Vol. 201, No. 0921-5107, pp.72–78.

Sönmezoğlu, S., Termeli, T.A., Akin, S. and Askeroğlu, I. (2013) 'Synthesis and characterization of tellurium-doped CdO nanoparticles thin films by sol-gel method', *Journal of Sol-Gel Science and Technology*, Vol. 67, No. 1, pp.97–104.

Tadjarodi, A. and Imani, M. (2011) 'A novel nanostructure of cadmium oxide synthesized by mechanochemical method', *Materials Research Bulletin*, November, Vol. 46, No. 11, pp.1949–1954.

Tannous, C. and Gieraltowski, J. (2008) 'The Stoner-Wohlfarth model of ferromagnetism', *European Journal of Physics*, Vol. 29, No. 3, pp.475–487.

Taufik, A., Tju, H., Prakoso, S.P. and Saleh, R. (2018) 'Different routes of synthesized CdO nanoparticles through microwave-assisted methods and photocatalytic study', *AIP Conference Proceedings*, Vol. 2023, No. 1, pp.020035, AIP Publishing LLC.

Tawfik, W.Z., Esmat, M. and El-Dek, S.I. (2017) 'Drastic improvement in magnetization of CdO nanoparticles by Fe doping', *Applied Nanoscience*, 1 November, Vol. 7, No. 8, pp.863–870.

Wolff, P.A., Bhatt, R.N. and Durst, A.C. (1996) 'Polaron-Polaron interactions in diluted magnetic semiconductors', *Journal of Applied Physics*, Vol. 79, No. 8 Part 2A, pp.5196–5198.

Yadav, I., Ahlawat, D.S. and Ahlawat, R. (2016) 'Cu-doped Cd1−x Zn x S alloy: synthesis and structural investigations', *Applied Physics A*, 2 March, Vol. 122, No. 3, pp.245.

Zhao, Z., Morel, D.L. and Ferekides, C.S. (2002) 'Electrical and optical properties of tin-doped CdO films deposited by atmospheric metalorganic chemical vapor deposition', *Thin Solid Films*, June, Vol. 413, Nos. 1–2, Nos. 1–2.